A Polarization Independent GaAs–AlGaAs Electrooptic Modulator

Ralph Spickermann, *Student Member, IEEE*, Matthew G. Peters, and Nadir Dagli, *Member, IEEE*

***Abstract*— Two designs for polarization independent GaAs–AlGaAs interferometric electrooptic modulators are described. One design uses the linear electrooptic effect to couple degenerate TE/TM eigenmodes of a single-mode waveguide. In the other design the eigenmodes need only be near degenerate. The design using the coupling between near degenerate TE/TM modes utilizes a novel biasing scheme. A novel polarization independent GaAs–AlGaAs interferometric optical modulator based on this design has been fabricated and characterized at 1.3 μm. This modulator is fabricated as a traveling wave modulator incorporating 50 Ω, phase velocity matched, low microwave loss electrodes for maximum electrical bandwidth.**

I. Introduction

POLARIZATION independent modulators are very attractive choices for fiber optic systems. However, to obtain polarization independent operation in guided wave devices using III–V compound semiconductors is difficult. The main difficulty is to get the same field induced refractive index change or absorption for both polarizations. Several recent approaches using tensile strained quantum wells achieved polarization independent operation in Mach–Zehnder [1] and directional coupler geometries [2]. By use of strained quantum wells the device can be made rather compact. However, temperature sensitivity, chirp, insertion loss, and growth requirements are possible difficulties. Another approach uses bulk electroabsorption to make intensity modulators [3]. This again results in compact devices, but insertion loss and temperature sensitivity issues still remain. On the other hand, the linear electrooptic effect can be used at wavelengths far away from the absorption edge and can result in low loss, chirp free operation. But the small electrooptic coefficient makes it difficult to make compact devices. Furthermore, it is difficult to utilize this effect to get the same index change for both polarizations. It is possible to use the linear electrooptic effect on [111] oriented substrates to make polarization independent directional coupler switches [4]. But it is difficult to obtain cleaved facets with [111] oriented substrates.

In this paper, we report a GaAs–AlGaAs traveling wave Mach–Zehnder electrooptic modulator that works for both TE and TM polarized light. This modulator uses the linear electrooptic effect on [100] oriented undoped substrates. Therefore, it has low loss and chirp free operation. Although the device is rather long it has the potential for very wide electrical bandwidth because it is a traveling wave design incorporating a phase velocity matched, 50-Ω characteristic impedance, low-loss electrode structure. This makes this device particularly suitable for analog microwave applications that require very wide small-signal electrical bandwidths and polarization independence. In the following sections, we first describe two approaches to make polarization independent modulators based on the linear electrooptic effect. This is followed by the experimental results on one of the approaches and a discussion and conclusions.

Manuscript received March 22, 1995; revised December 26, 1995. This work was supported in part by the ARPA Optoelectronic Technology Center (OTC) and a UC/MicroTektronix Grant.

The authors are with the Electrical and Computer Engineering Department, University of California, Santa Barbara, CA 93106 USA.

Publisher Item Identifier S 0018-9197(96)03199-5.

II. Principle of Device Operation

Top view and cross-sectional schematics of the device are shown in Fig. 1. The wafer is a [100] MBE grown unintentionally doped GaAs–AlGaAs heterostructure. The heterostructure is almost self depleting because of surface Fermi level pinning and depletion originating at the semi-insulating substrate interface. The optical structure is a Mach–Zehnder interferometer made out of single-mode rib waveguides. The electrode structure is a specially designed 50-Ω impedance coplanar waveguide that is phase velocity matched with the optical guides [5], [6].

The electrodes make Schottky contacts with the heterostructure. When a differential voltage is applied between two adjacent electrodes, two back-to-back Schottky diodes are biased. This creates a depleted region with a large electric field over the optical guide between them. As shown in Fig. 1(b) this electric field is predominantly horizontal in the optical guides between the electrodes, that is, [011] directed. This perturbs the index ellipsoid through the electrooptic effect. The major and minor axes of the resultant index ellipsoid are at 45° with respect to the main electric field components of the TE and TM eigenmodes of the optical waveguide as illustrated in Fig. 1(b) [7], [8]. Furthermore, the index increase Δn along the major axis of the index ellipsoid is exactly the same as the index decrease along minor axis such that

$$|\Delta n| = \tfrac{1}{2}\left(n^3 r_{41}|E|\right) \tag{1}$$

where n is the index of refraction, r_{41} is the electrooptic coefficient, and E is the applied electric field. This index ellipsoid perturbation acts to couple the TE and TM eigenmodes of the unperturbed waveguide due to the presence of the off-axis index ellipsoid components.

Coupled mode theory can be used to describe this situation [9]. It gives two values of propagation constant β for this

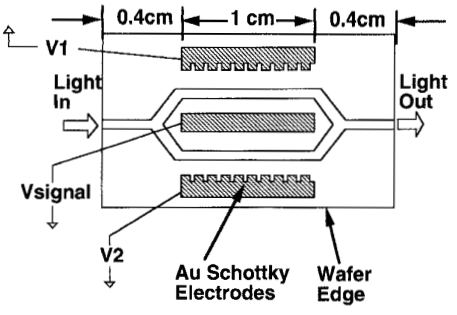

(a)

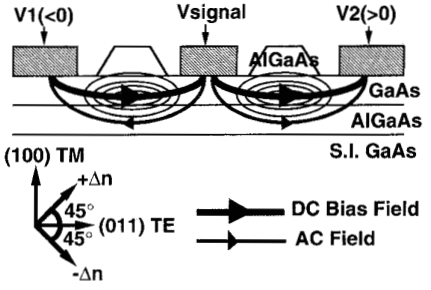

(b)

Fig. 1. (a) Overhead schematic view of the device. The electrooptic interaction length is 1 cm. (b) Cross-sectional schematic of the device illustrating horizontal fields through the optical guides. The major and minor axes of the resultant index ellipsoid with respect to the main electric field components of the TE and TM modes of the optical waveguide for a [011] oriented electric field are illustrated.

coupled mode system, which are

$$\beta = \frac{\beta_{\mathrm{TE}} + \beta_{\mathrm{TM}}}{2} \pm \sqrt{\left(\frac{\beta_{\mathrm{TE}} - \beta_{\mathrm{TM}}}{2}\right)^2 + \kappa^2}. \qquad (2)$$

Here $\beta_{\mathrm{TE}}, \beta_{\mathrm{TM}}$ are the unperturbed propagation constants of the TE and TM modes respectively and κ is the coupling constant. κ is proportional to the applied electrode field and can be expressed as [9]

$$\kappa = (\pi/\lambda) n^3 r_{41} E. \qquad (3)$$

Using (2), the perturbations to TE and TM propagation constants can be written as

$$\begin{aligned} \Delta\beta_{\mathrm{TE}} &= -\delta + \sqrt{\delta^2 + \kappa^2} \\ \Delta\beta_{\mathrm{TM}} &= +\delta - \sqrt{\delta^2 + \kappa^2} \end{aligned} \qquad (4)$$

where

$$\delta = \frac{\beta_{\mathrm{TE}} - \beta_{\mathrm{TM}}}{2} \qquad (5)$$

is the "detuning" parameter and is a measure of the phase velocity mismatch between the TE and TM eigenmodes. The magnitude of the propagation constant perturbation is the same for both TE and TM polarizations, so $|\Delta\beta_{\mathrm{TE}}| = |\Delta\beta_{\mathrm{TM}}| = |\Delta\beta|$ as seen in (4). This change as a function of κ is plotted in Fig. 2 with $|\delta|$ as a parameter.

In addition to this propagation constant perturbation, coupled mode theory predicts transfer of energy between the TE and TM eigenmodes. This is governed by the expression

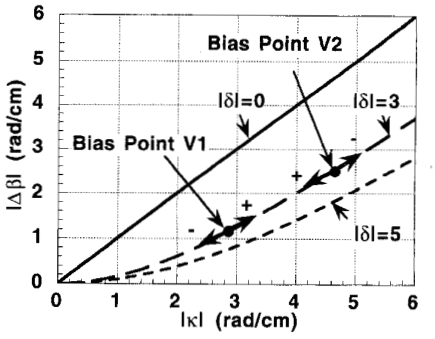

Fig. 2. Magnitude of propagation constant perturbation $|\Delta\beta|$ as a function of coupling constant magnitude $|\kappa|$ for different detuning parameter magnitudes $|\delta|$. The arrows on the $|\delta| = 3$ plot show the action in each arm around its bias point for the indicated signal voltage polarity on the center electrode.

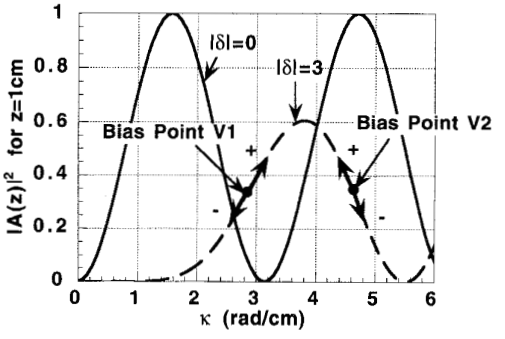

Fig. 3. Fractional eigenmode power conversion magnitude $|A(z)|^2$ after 1 cm as a function of coupling constant κ with $|\delta|$ as a parameter. The arrows show the action in each arm around its bias point for the indicated signal voltage polarity on the center electrode.

$$A(z) = -ie^{-i\delta z} \frac{\kappa}{(\kappa^2 + \delta^2)^{1/2}} \sin\left[((\kappa^2 + \delta^2)^{1/2})z\right] \qquad (6)$$

where $A(z)$ is the normalized amplitude of one of the eigenmodes as a function of coupling length z [9]. Normalized power of one of the eigenmodes, $|A(z)|^2$, as a function of κ with $|\delta|$ as a parameter is shown in Fig. 3. As $|\delta|$ gets smaller the TE/TM eigenmodes become more degenerate and the propagation constant perturbation (Fig. 2) and the power transfer between the TE/TM modes (Fig. 3) become more efficient.

In order to illustrate the polarization independent modulator operation based on this coupling, first consider the degenerate TE/TM eigenmode case $\delta = 0$. Here $A(z) = -i\sin(\kappa z)$ and complete mode conversion is possible. This modulator would be operated by keeping the outer conductors at ground potential [$V_1 = V_2 = 0$ in Fig. 1(b)] and applying a signal voltage to the center conductor. The resulting electric fields in the interferometer arms are then equal in magnitude but opposite in direction. Therefore the κ's in the arms are of opposite sign since κ is directly proportional to the electric field as seen in (3). Assume that $\kappa L = \pi/2$, where L is the length of the electrode. In this case, an incoming TE(TM) polarized mode is completely converted to an TM(TE) polarized mode in both arms. But since the amplitude of the converted eigenmode

$A(z)$ is sensitive to the sign of κ, the modes at the ends of the arms are of opposite phase. Therefore, when combined at the output, a TE(TM) polarized input excites the first higher order TM(TE) mode that radiates in the single-mode output section. So the modulator works just like a regular Mach–Zehnder modulator except that the higher order radiation mode excited in the output is of the opposite polarization than the input excitation. For $0 \leq \kappa L \leq \pi/2$ different degrees of modulation are achieved and the polarization of the output will be the same as the polarization of the input. This is very similar to the scheme proposed in reference [10] utilizing a special electrode geometry in $LiNbO_3$. However, in the case of GaAs the implementation is different because of the different form of the index ellipsoid.

It is interesting to note that if the electric field is applied in the [100] (vertical) direction, regular Mach–Zehnder operation for TE polarization only results. Under push-pull operation the electric field required to turn this polarization dependent modulator completely off can be calculated using $(2\pi/\lambda)\Delta nL = \pi/2$ where $|\Delta n| = \frac{1}{2}(n^3 r_{41}|E|)$, which is the same as the index perturbation for a [110] directed electric field. Combining these two conditions one obtains $|E| = \lambda/(2Ln^3 r_{41})$, which is the same field required to turn off the polarization independent modulator determined using $\kappa L = \pi/2$ where κ is given in (3). Therefore, in a III–V compound semiconductor Mach–Zehnder, when $\delta = 0$ an electric field applied in [110] direction generates a polarization independent operation with the same efficiency as the resulting TE only operation when the same electric field is applied in [100] direction.

In practice, the δ of an optical waveguide depends on the geometry of the guide. By proper design, it is possible to fabricate optical guides with $|\delta| \leq 2$ rad/cm. However, even for such low $|\delta|$ values the described mode of operation will yield modulators with poor extinction ratio since the light that is not polarization converted passes through unaffected. But a different approach can be employed to eliminate this difficulty as described next.

This approach utilizes the phase constant perturbation $\Delta\beta$ shown in Fig. 2 together with the mode conversion effect of Fig. 3. To illustrate this, consider the $|\delta| = 3$ case as an example. As seen in (2), for phase constant perturbation only the magnitude of κ (equivalently the magnitude of the electric field) is relevant. Therefore, to create a differential phase shift between the arms, the magnitudes of the electric field in the arms of the interferometer should be modified with respect to one another. The biasing scheme shown in Fig. 1(b) achieves this. The dc biases on the outer conductors generate electric fields of differing magnitude but the same direction in the arms. These dc-bias generated $|\kappa|$'s and their effect are indicated in Figs. 2 and 3. When a modulating signal is applied to the signal electrode, the magnitude of the electric field will decrease in one arm and increase in the other. This decreases the phase constant perturbation $\Delta\beta$ in one arm and increases it in the other as shown in Fig. 2. The same differential phase shift is created between the arms for both polarizations since $\Delta\beta$ is polarization independent. At the same time the polarization conversion in the arms will also change. But if the dc-bias voltages are adjusted such that the $|\kappa|$'s are around a local point of symmetry as shown in Fig. 3, the change of polarization conversion will be nearly the same in both arms. This assures that equal amounts of each eigenmode will be present at the output for maximum interference. The efficiency of this modulator is the differential phase shift generated as a function of applied voltage. This depends on the slope of the $\Delta\beta$ versus $|\kappa|$ curve of Fig. 2. As long as $|\delta|$ is not too large efficiency is very close to that of $\delta = 0$ case for which the slope is 1. For example, even for $\delta = 5$ at $|\kappa| = 5$ the slope is 0.71, which indicates that this mode of operation will require a 40% increase in the operating voltage compared to TE only operation or polarization independent operation when $\delta = 0$.

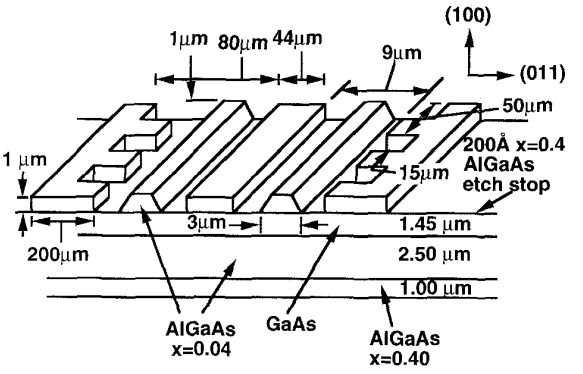

Fig. 4. Schematic of the modulator electrooptic interaction region.

III. Experimental Results

The dimensions of the interaction region of the fabricated device are illustrated in Fig. 4. The vertical structure is MBE grown on a semi insulating GaAs substrate and is unintentionally doped. It consists of a 1-μm-thick top cladding $Al_{0.04}Ga_{0.96}As$ layer on a 1.45-μm-thick GaAs core, which is on top of a 2.5-μm-thick $Al_{0.04}Ga_{0.96}As$ bottom cladding layer. Beneath this is an $Al_{0.40}Ga_{0.60}As$ layer to prevent leakage of the mode into the substrate. This layer was utilized to minimize the thickness of the bottom $Al_{0.04}Ga_{0.96}As$ layers so that the entire structure is more readily depleted. The optical guides are rib waveguides of trapezoidal shape with base widths of 3 μm. The height of the rib is 1 μm and is controlled using a 200-Å-thick $Al_{0.40}Ga_{0.60}As$ etch stop layer. This allows the precise control of the guide geometry, which is essential to get a predictable δ value.

Fabrication consisted of two steps. First the optical guides were etched in a citric acid based solution which etches the $Al_{0.40}Ga_{0.60}As$ layer very slowly and hence effectively stops on this layer [11]. Next Ti–Pt–Au 200 Å/200 Å/1 μm-thick electrodes were lifted off. The resultant electrode geometry is a specially designed slow wave coplanar line [5], [6]. The measured phase velocity versus frequency of this coplanar line is shown in Fig. 5. The phase velocity is matched to within 1% of the phase velocity of the optical wave up to at least 40 GHz. The characteristic impedance was measured to be 50 $\pm$ 5 Ω and the loss was 4.6 dB/cm at 40 GHz. Due to very close phase velocity matching the modulator bandwidth is limited

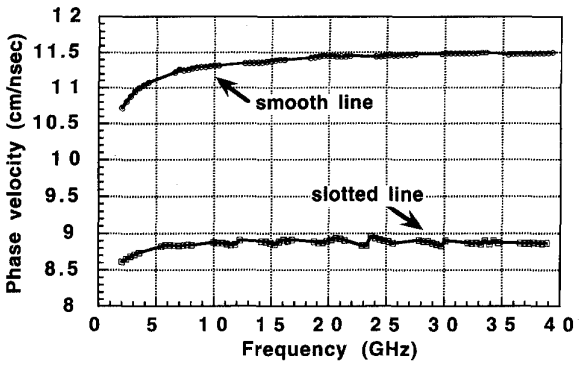

Fig. 5. Measured microwave phase velocity versus frequency for the coplanar slow wave modulator electrodes. The phase velocity of 1.3-μm light in GaAs is 8.8 cm/ns. Also shown is the corresponding phase velocity for a smooth coplanar line to illustrate the amount of phase velocity slowing achieved.

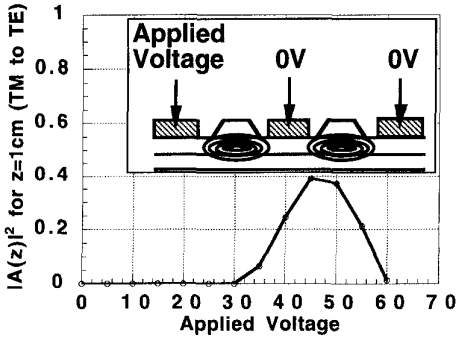

Fig. 6. Measured fractional eigenmode power conversion magnitude $|A(z)|^2$ in a 1-cm-long modulator arm. The corresponding $|\delta|$ is approximately 6 rad/cm.

by the electrode microwave loss and the measured loss values predict a modulator bandwidth of at least 40 GHz. Indeed for TE only modulators using this electrode design bandwidths in excess of 40 GHz have been recently demonstrated [12], [13].

The optical measurements were done by end fire coupling a 1.3-μm DFB laser of known polarization into the input facet of the device with a microscope objective. The output was focused onto a detector with another microscope objective through an adjustable width slit to spatially filter out the optical mode from the stray background light. The single pass optical loss of the entire 1.8-cm-long structure was measured to be at most 6 dB using to the method outlined in [14].

The $|\delta|$ was determined by measuring the fractional mode conversion in one arm of the interferometer. This is done by applying a voltage to the corresponding outer conductor while the other two electrodes are kept grounded. The result shown in Fig. 6 indicates a $|\delta|$ of $\sim$6 rad/cm. Beam propagation method modeling based on [15] indicated a $|\delta|$ of 5 rad/cm which is close to the measured value.

In the experiments we investigated analog applications in which a sinusoidal signal is the modulating signal. We also want the optical response of the modulator in phase with the sinusoidal modulating signal. Therefore, the maximum of the applied signal, $V_{\max}$, should correspond to the modulator on state. This requires $\Delta\beta$ or κ to be the same in both arms. This means that the magnitude of the voltage difference between the two arms should be the same to keep the arms balanced. Arbitrarily assuming $V_1 < 0$ and $V_2 > 0$ and using Fig. 2, we obtain $|V1| + V_{\max} = V2 - V_{\max}$.

Again, to keep the modulator response in phase with the modulating signal we want the minimum of the applied signal, $-V_{\max}$, to correspond to the modulator off state. Then, based on Fig. 2, the voltages across the arms are $|V1| - V_{\max}$ and $V2 + V_{\max}$. The magnitude of these voltages determine the κ and $\Delta\beta$ values on both arms. We want the $\Delta\beta$ difference between the two arms π. Since $|\delta|$ was high and the electrode gap of 9 μm was large we could not obtain the required π phase difference between the arms. Therefore, we tried to maximize the $\Delta\beta$ difference between the arms to get as close to π as possible. Since $|V1| - V_{\max}$ is the lower magnitude we chose it to be the lowest possible value, which is zero. The maximum $V2 + V_{\max}$ can ever get is limited by the breakdown voltage, V_B, of the Schottky electrodes. If this value is exceeded excessive current injection into the optical guides will occur, which could create additional index charge do to carrier injection and heating. The maximum reverse electrode current limit was chosen to be 100 μA. This occurred at a voltage difference of 70 V. If we combine these three conditions, namely $|V1|+V_{\max} = V2-V_{\max}$, $|V1|-V_{\max} = 0$ and $V2 + V_{\max} = V_B$ we obtain $|V1| = V_B/4 \approx 17$ V, $V2 = 3V_B/4 \approx 51$ V, and $V_{\max} = V_B/4 \approx 17$ V.

These bias values maximize the $\Delta\beta$ difference between the arms. However, we do not get the same degree of TE/TM conversion in both arms. This is because we are not biased around the symmetry of the power transfer characteristics shown in Fig. 3. This combined with less than $\pi\Delta\beta$ difference makes off state less than ideal and reduces the on/off ratio.

The TM large signal responses with no bias and with maximum extinction ratio biases applied are shown in Fig. 7. These bias values are close to the ideal ones calculated above. Due to different bias voltages on the arms there is a built in phase shift for both polarizations. That is why when the signal voltage is zero the light output is about 65% of its maximum value. For one polarity of the applied signal the phase shift between the arms for both polarizations decreases, thus increasing the light output. For the opposite signal voltage polarity, the phase shift increases and the light output decreases. This is consistent with the desired mode of operation. The large $|\delta|$ value resulted in the larger than expected operating voltage. The 9 μm gap between the electrodes is another important factor responsible for large drive voltages required. As described earlier this also resulted in an on/off ratio of only 5 : 1 since the relative amounts of TE and TM polarizations in the arms was not balanced as well as the relative phase shift between the arms was less than π.

In this mode of operation one should not see any modulation with no bias applied. The slight modulation observed with no bias in Fig. 7 is due to the Fabry–Perot effect originating from the cleaved facets of the modulator. Although the applied signal to the center conductor with no bias does not create a differential phase shift between the arms, it creates an overall $\Delta\beta$ in both arms. This changes the electrical length of the Fabry–Perot cavity resulting in the observed modulation

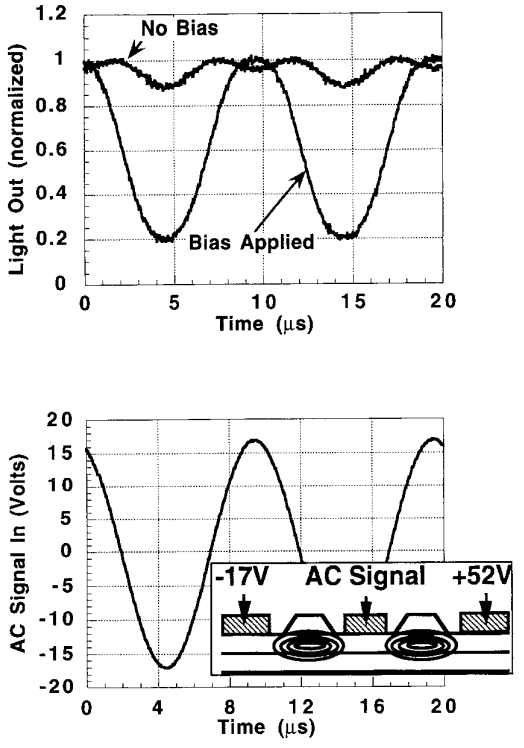

Fig. 7. Large-signal TM response of the modulator measured at 100 kHz.

characteristics. This result is consistent with the observed single-pass loss of the device. This undesired modulation will be eliminated when the facets are anti-reflection coated as in any realistic operation.

Fig. 8 is a comparison of the optimal TE and TM transfer functions that are very close to one another. The TE-bias voltages for optimal extinction ratio are slightly different than for TM. This is mainly due to the electrode employed. Along the 9-μm-wide section of the electrode the small vertical component of the electric field does not contribute to the TE response due to its odd symmetry over each optical waveguide. However, along the periodic slots of the electrode this odd symmetry no longer exists, hence a small vertical component of the electric field creates a differential phase shift for the TE polarization. This is not a big contribution since slots exist only over 30% of the electrode, and the field is quite weak on the slotted sections. Nevertheless the electrode is long enough to make the modulation of the TE polarized input slightly more efficient. This additional contribution to TE polarization also necessitates changing the bias values slightly to make the on state of the modulator coincide with the peak of the modulating signal. However, this is not a fundamental property of this approach and is an artifact of the electrode geometry employed.

IV. Conclusion

In this paper, two possible designs of polarization independent modulators utilizing only the linear electrooptic effect were given. A polarization independent electrooptic modulator using one of these approaches was demonstrated.

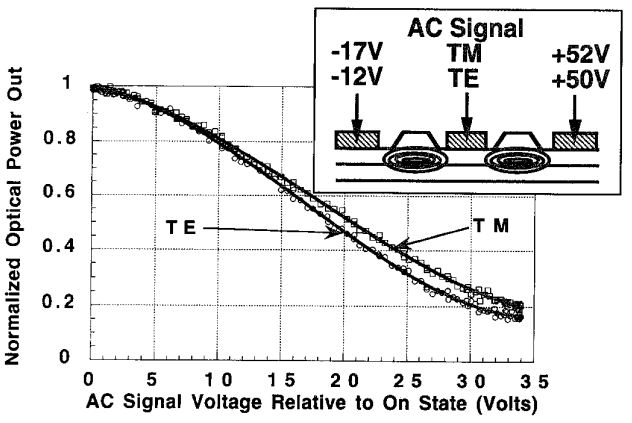

Fig. 8. TE and TM large-signal transfer functions of the modulator at 100 kHz.

This modulator operates by controlling the coupling between near degenerate TE/TM modes and the propagation constant perturbation created by this coupling. This control is possible through a novel biasing scheme, which changes the magnitude of the field in both arms of the interferometer in a push–pull fashion. The observed on/off ratio was low due to relatively large phase velocity mismatch between the TE and TM eigenmodes. This combined with the large electrode gap resulted in high operation voltage. However, polarization independent operation was achieved, demonstrating the feasibility of the idea.

References

[1] J. E. Zucker *et al.*, "Strained quantum wells for polarization independent electrooptic waveguide switches," *J. Lightwave Technol.*, vol. 10, pp. 1926–1930, Oct. 1992.

[2] T. Aizawa, Y. Nagasawa, K. G. Ravikumar, and T. Watanabe, "Polarization independent switching operation in directional coupler using tensile strained multi quantum well," *IEEE Photon. Technol. Lett.*, vol. 7, no. 1, pp. 47–49, Jan. 1995.

[3] G. Mak, C. Rolland, K. E. Fox, and C. Blaauw, "High speed bulk InGaAsP/InP electroabsoption modulators with bandwidth in excess of 20 GHz," *IEEE Photon. Technol. Lett.*, vol. 2, no. 10, pp. 730–733, Oct. 1990.

[4] K. Komatsu *et al.*, "Polarization independent GaAs/AlGaAs electrooptic guided wave directional coupler switch using [111] oriented GaAs substrate," *OSA Proc. Photon. Switch.*, vol. 8, pp. 24–27, 1991.

[5] R. Spickermann and N. Dagli, "Millimeter wave coplanar slow wave structure on GaAs suitable for use in electrooptic modulators," *Electron. Lett.*, vol. 29, no. 9, pp. 774–775, Apr. 1993.

[6] ——, "Experimental analysis of millimeter wave coplanar waveguide slow wave structures on GaAs," *IEEE Trans. Microwave Theory Tech.*, vol. 42, no. 10, pp. 1918–1924, Oct. 1994.

[7] S. Namba, "Electro-optical effect of zincblende," *J. Opt. Soc. Amer.*, vol. 51, no. 1, pp. 148-151, Jan. 1961.

[8] S. Y. Wang and S. H. Lin, "High speed III–V electrooptic modulators at $\lambda = 1.3\mu$m," *J. Lightwave Technol.*, vol. 6, pp. 758–771, June 1988.

[9] A. Yariv, *Introduction to Optical Electronics*, 2nd ed. New York: Holt, Rinehart, and Winston, 1976.

[10] H. F. Taylor, "Polarization independent guided wave optical modulators and switches," *J. Lightwave Technol.*, vol. 3, pp. 1277–1280, Dec. 1985.

[11] C. Juang, K. J. Kuhn, and R. B. Darling, "Selective etching of GaAs and $Al_{0.30}Ga_{0.70}As$ with citric acid/hydrogen peroxide solutions," *J. Vac. Sci. Technol. B*, vol. 8, pp. 1121–1124, Sept./Oct. 1990.

[12] R. Spickermann, N. Dagli, and M. G. Peters, "GaAs/AlGaAs Electrooptic Modulator with Bandwidth >40 GHz," *Electron. Lett.*, vol. 31, no. 11, pp. 915–916, May 1995.

[13] ——, "A GaAs/AlGaAs Mach–Zehnder electrooptic modulator with electrical bandwidth in excess of 40 GHz," presented at the 1995 Optical Fiber Commun. Conf., San Diego, CA, Feb.–Mar. 1995, paper Thk6.

[14] R. G. Walker, "Simple and accurate loss measurement technique for semiconductor optical waveguides," *Electron. Lett.*, vol. 21, no. 13, pp 581–583, 1985.
[15] Y. Chung, N. Dagli, and L. Thylen, "An explicit finite difference vectorial beam propagation method," *Electron. Lett.*, vol. 27, no. 23, pp. 2119–2120, Nov. 1991.

Ralph Spickermann (S'89) was born March 3, 1965, in Santa Clara, CA. He received the B.S. degree in electrical engineering and computer science from the University of California at Berkeley and the M.S. degree in electrical engineering from the University of California at Santa Barbara, in 1986 and 1991, respectively, and is currently pursuing the Ph.D. degree at the U.C. Santa Barbara.

From 1986 to 1989, he was employed at Teledyne MEC in Palo Alto, CA, where he worked on the design and production of traveling wave tubes for radar and satellite communications applications.

Matthew G. Peters, photograph and biography not available at the time of publication.

Nadir Dagli (S'77–M'87) was born in Ankara, Turkey. He received the B.S. and M.S. degrees in electrical engineering from Middle East Technical University, Ankara, Turkey, in 1976 and 1979, respectively, and the Ph.D. degree in electrical engineering from the Massachusetts Institute of Technology, Cambridge, MA, in 1986. His Ph.D. research focused on the design, fabrication, and modeling of guided-wave integrated optical components in III-V compound semiconductors. He also worked on III-V materials preparation by LPE and the modeling and analysis of heterojunction bipolar transistor for microwave and millimeter-wave applications.

After graduation he joined the electrical and computer engineering department at University of California at Santa Barbara, where he is currently an Associate Professor. His current interests are design, fabrication and modeling of guided-wave components for optical integrated circuits, especially ultrafast electrooptic modulators and WDM components, calculations on the optical properties of quantum wires, experimental study of novel quantum devices based on ballistic transport in quantum wires.

Dr. Dagli was awarded NATO science and IBM predoctoral fellowships during his graduate studies. He is the recipient of 1990 UCSB Alumni Distinguished Teaching Award and 1990 UC Regents Junior Faculty Fellowship and is a member of IEEE. He was a member of the Subcommittee on Modeling, Numerical Simulation and Theory of Integrated Photonics Research Topical Meeting, 1992–1995. He chaired the same subcommittee in 1994. Since 1994 he is serving as a member of the Integrated Optics and Optoelectronic Committee of IEEE Lasers and Electro Optics Society Annual Meeting.